



Amine-modified magnetic particles: An efficient tool for enhanced RNA extraction

Petra Vopařilová^a, Zbyněk Šplíchal^a, Pavel Švec^a, Pavel Kulich^b, Ondřej Malina^c,
Michal Otyepka^{c,d}, Ondřej Zítka^a, Jiří Kudr^{a,*}

^a Department of Chemistry & Biochemistry, Mendel University in Brno, Zemědělská 1, 61300 Brno, Czech Republic

^b Veterinary Research Institute, Hudcova 296/70, 621 00 Brno, Czech Republic

^c Regional Centre of Advanced Technologies and Materials, The Czech Advanced Technology and Research Institute (CATRIN), Palacký University Olomouc, Šlechtitelů 27, 779 00 Olomouc, Czech Republic

^d IT4Innovations, VSB – Technical University of Ostrava, 17. listopadu 2172/15, 708 00 Ostrava-Poruba, Czech Republic

ARTICLE INFO

Editor: Raquel Aires Barros

Keywords:

Extraction
Isolation
Nanoparticles
Nucleic acid
Purification
Silica
Silicate
Amine

ABSTRACT

Magnetic particles are an effective tool for simple, time-saving, and labour-saving nucleic acid extraction. In this study, we investigated the isolation of nucleic acids (NA) using 11 variants of magnetic nanoparticles (MPs, 52 ± 6.8 nm) with a surface concentration of amine groups up to $20.8 \text{ nmol} \cdot \text{mg}^{-1}$. All results were compared with morphologically identical magnetic material modified with SiO_2 grafted with (3-aminopropyl)triethoxysilane (APTES). The properties of these materials were characterized by transmission electron microscopy, scanning electron microscopy, dynamic and electrophoretic light scattering, and magnetometry. Concentrations of amine groups on MPs-APTES were determined by the chemical bind and release method with photometric quantification.

The isolation potential of the proposed materials toward NAs was evaluated using gel electrophoresis with photometric determination of NAs concentrations and RT-qPCR. Our results show that the NAs yields of MPs-APTES are higher than the reference MPs- SiO_2 , regardless of the amine group concentrations. Although the total yield decreased with the concentration of amine groups, a different affinity towards genomic DNA (gDNA) was observed. A high concentration of grafted amine groups induced a preference for ribosomal RNA (rRNA) over gDNA and mediated effective NA elution. Densitometric image analysis of gDNA bands showed that NAs isolated by MPs- SiO_2 contained significantly higher DNA levels than MPs with 1/32 %, 1/2 %, and 16 % APTES modification, which was subsequently confirmed by qPCR. Gene expression analysis performed by RT-qPCR revealed that unwanted gDNA contamination did not significantly affect the threshold cycles (Ct) of target genes when cDNA-specific primers were used, but may lead to overestimation when targeting genes with low expression and no possibility to design cDNA-unique primers. From a practical point of view, MPs-APTES provided better dose-dependent NA isolation performance with stable NA quality.

1. Introduction

In molecular biology and diagnostics, nucleic acid (NA) extraction and purification are critical for downstream applications like PCR, sequencing, and cloning [1]. The purity and quality of NAs are essential for accurate genomic testing results. High-quality RNA is crucial for RT-qPCR, transcriptome analysis, northern blotting, cloning, RNA sequencing, and *in situ* hybridization, requiring both purity and integrity for accurate analyses.

RNA extraction methods primarily involve fluid-phase and solid-phase techniques. Both require specimen homogenization and lysis to release RNAs, followed by isolation and purification from cell debris and components like salts and RNases. Commonly used chemicals, such as guanidinium salts and sodium dodecyl sulfate, denature RNases and dissolve cellular components. Extensive purification is needed to remove these chemicals as they can inhibit downstream applications [2–4].

Fluid-phase extraction uses acid guanidinium isothiocyanate (GITC), phenol, and chloroform for phase separation but often requires

* Corresponding author.

E-mail address: kudr@mendelu.cz (J. Kudr).

<https://doi.org/10.1016/j.seppur.2024.129788>

Received 1 July 2024; Received in revised form 17 September 2024; Accepted 18 September 2024

Available online 28 September 2024

1383-5866/© 2024 The Author(s). Published by Elsevier B.V. This is an open access article under the CC BY-NC license (<http://creativecommons.org/licenses/by-nc/4.0/>).

optimization and is not suitable for automation [5]. Solid-phase extraction, however, is rapid and effective, relying on the interaction between the solution and solid sorbent, with silica surfaces and anion exchange membranes commonly used [6,7].

Silica-based extraction is popular due to its simple bind-wash-elute process. In the presence of chaotropic salts, NAs bind to silica while proteins and salts are removed by washing [8]. The interaction mechanisms include hydrogen bonds, hydrophobic interactions, and electrostatic interactions, influenced by conditions like pH, NA type, and ionic concentration [9–16]. Silica binds all NA types, with single-stranded DNA (ssDNA) binding preferentially over double-stranded DNA (dsDNA) [9]. Pretreatment with RNase A or DNase I ensures selectivity for DNA or RNA but increases costs [17]. NAs sorbents are used in spin columns, benefiting from centrifugal or vacuum systems. Magnetic materials offer a labor-efficient alternative, with core-shell structures allowing manipulation via external magnetic fields. These materials provide a high surface-to-volume ratio, enhancing extraction and purification efficiency [18,19].

In this study, we fabricated MPs with different amounts of amine groups on their surface. We systematically examined their potential for DNA and RNA isolation from cell lysates. Further, we compared the yield of extracted RNA as a function of the amount of APTES on the MPs surface, where SiO₂ modified MPs represent reference material. In addition, the level of gDNA contamination in NA extracts was assessed using densitometric analysis and qPCR. Finally, the impact of NAs isolated from MPs with and without APTES modification on RT-qPCR results was determined.

2. Materials and methods

2.1. Chemicals

FeSO₄·7 H₂O, KNO₃, NH₄OH (28–30 % NH₃ basis), H₂SO₄ (95–98 %), tetraethyl orthosilicate (TEOS), and 3-aminopropyltriethoxy silane (APTES) and other chemicals were purchased from Sigma-Aldrich (St. Louis, MO, USA) in ACS purity and were used as received. Potassium hydroxide (1 M) was ordered from Supelco (Bellefonte, PA, USA). All water-based solutions were prepared using milli-Q water (resistivity higher than 18.2 MΩ • cm at 25 °C) from Millipore, unless stated otherwise (Burlington, MA, USA).

2.2. Magnetic particles synthesis and modification

Magnetic particles were synthesized using the modified method proposed by Sugimoto and Matijevic [20]. In detail, 34.751 g of FeSO₄ · 7 H₂O was dissolved within 150 mL of water with the addition of 15 μL of sulfuric acid. The solution was subsequently degassed. Within a 5 L reagent flask, 4.3 L of mQ water, 101.103 g of KNO₃, and 500 mL of 1 M KOH were added and the solution was degassed as well. Both solutions were mixed together in a reagent flask, covered with a cap, and transferred within a water bath preheated to 90 °C and left there for 3 h. The obtained magnetic solid was washed thoroughly using a permanent magnet. Subsequently, particles were dispersed within 1 L of 0.5 M sodium citrate water solution and incubated in a water bath at 80 °C for 1 h. The obtained magnetic cores were washed thoroughly using a permanent magnet and used for modification.

The magnetic particles were modified with a SiO₂ layer using a modified Stöber method, where the ethoxy groups of TEOS are hydrolyzed in a mixture of distilled water and ethanol in the presence of ammonia as a reaction catalyst. More precisely, 4 g of magnetic cores (dry solid) were dispersed within a mixture of 700 mL of water, 1000 mL of pure ethanol, and 51 mL of ammonium hydroxide solution using sonication. The solution was stirred with an overhead stirrer and 20 mL of TEOS was added slowly. The solution was stirred for 20 h. The resulting material denoted as MPs-SiO₂ was washed with ethanol and water using a magnet and dispersed within the water. The concentration

of MPs-SiO₂ was determined by weighing the dry solid of aliquote.

Amino groups were introduced onto magnetic cores modified with a SiO₂ layer using various amounts of APTES. Each variant was modified as follows, 200 mg of MPs-SiO₂ were dispersed within 100 mL of water and 100 mL of pure ethanol using a sonicator. The solution was subsequently transferred to an overhead stirrer and 0.063, 0.13, 0.25, 0.50, 1.0, 2.0, 4.0, 8.0, 16.0, and 32.0 mL of APTES were added slowly within each individual variant. The resulting solutions were stirred for 20 h and subsequently thoroughly washed with ethanol and water, respectively. Variants are denoted as MPs-APTES 1/32 %, MPs-APTES 1/16 %, MPs-APTES 1/8 %, MPs-APTES 1/4%, MPs-APTES 1/2 %, MPs-APTES 1 %, MPs-APTES 2 %, MPs-APTES 4 %, MPs-APTES 8 % and MPs-APTES 16 %, respectively. The concentration of each MPs-APTES samples were determined by weighing the dry solid of an aliquot of known volume.

2.3. Amine groups quantification

Amine groups on the surface of MPs-APTES variants were determined using 4-nitrobenzaldehyde (4-NBA) assay [21]. In detail, 1 mg of particles were dispersed within a 4-NBA solution (1 mg mL⁻¹) in 1 mL of methanol with 0.8 % glacial acetic acid. Dispersion was incubated in the rotator for 3 h. Subsequently, the particles were 4-times washed using a magnet and methanol with 0.8 % glacial acetic acid. 4-NBA, which reacted with particles surface amino groups, were eluted to 250 μL of solution prepared by mixing 75 mL of ethanol, 75 mL of water, and 200 μL of glacial acetic acid. Eluted 4-NBA was quantified using photometric determination at 275 nm and calculated using a 4-NBA calibration curve. The obtained data were expressed as molar amount of amine groups per mg of MPs.

2.4. Microscopic analysis and energy-dispersive X-ray spectroscopy

SEM images of MPs were taken on MIRA 2 SEM from Tescan (Brno, Czech Republic) using ultra high resolution mode. Micrographs were obtained using the In-Beam secondary electron (SE) detector at a 3 mm working distance and 15 kV acceleration voltage. The measurement was performed at a high vacuum. Elemental analysis was made on energy dispersive X-ray (EDX) detector X-MAX 50 (Oxford instruments PLC, Abingdon, UK) with the same condition as photos (high vacuum, accelerating voltage 15 kV). Only the work distance was different (15 mm) and the Everhart–Thornley SE detector was used. The power of the detector was set so that the input signal was about 19,000–21,000 counts. At this setting, the output signal was about 15,000–16,000 counts, and detector deadtime fluctuated between 19–21 %. The time for each analysis was 20 min. The spot size was 100 nm.

2.5. Transmission electron microscopy of MPs

The powder of magnetic nanoparticles was put into a grid-coated formvar film (300 Old Mesch, Agar Scientific, Stansted, United Kingdom). The grid prepared in this way was observed under a transmission electron microscope Philips 208 S Morgagni (FEI, Hillsboro, OR, USA) at 14,000–180,000 × magnification and an accelerating voltage 80 kV.

The particle size distribution analysis was performed using ImageJ software (<https://www.imagej.net>). From obtained cross-sectional areas of analysed MPs, diameters of circularly shaped particles were expressed in histograms.

2.6. Zeta potential analysis

Particle zeta potential were determined by electrophoretic light scattering (ELS) method by Zetasizer Nano-ZS (Malvern Instruments Ltd., Worcestershire, UK) with a scattering angle $\theta = 173^\circ$. Samples were measured in 10 mM KCl solution.

2.7. Magnetometry

The magnetic data were measured on powder samples using a Dynacool Physical Properties Measurement System (PPMS) from Quantum Design (San Diego, CA, USA) with the VSM option. The experimental data were corrected for the diamagnetism and signal of the sample holder.

2.8. Cell lines and culture conditions

A human breast cancer cell line established from the pleural effusion of ductal carcinoma (T47D), was used in this study. The cell line was purchased from the American Type Culture Collection (ATCC, Manassas, VA, USA). The cells were cultured in RPMI 1640 with 10 % of fetal bovine serum (FBS) and the culture media was supplemented with an antibiotic mixture (penicillin (100 U mL⁻¹) and streptomycin (0.1 mg mL⁻¹). The cells were grown and preserved *in vitro* for 48 h at a constant temperature of 37 °C, 5 % CO₂, and 100 % humidity in an incubator Galaxy® 170 R (Eppendorf, Hamburg, Germany). Subsequently, the cells were transferred into a new 50 mL centrifuge tube and centrifuged at 1200 rpm for 5 min at 25 °C. The supernatant was carefully removed, and the cell pellet was re-suspended and washed twice with 1 mL of PBS buffer. A 10 µL aliquot sample of cell mixture was then retrieved and mixed with 10 µL of trypan blue (Thermo Fisher Scientific, Waltham, MA, USA). The mixture was then loaded into a Countess II FL Automated Cell Counter AMQAF1000 (Thermo Fisher Scientific, Waltham, MA, USA), and a cell count was calculated. The cell mixture was then re-suspended in lysis/binding buffer (pH 6.6, 4.5 M GITC, 50 mM Tris-HCl, 30 % Triton X-100) into new 1.5 mL centrifuge tubes containing approximately 5 · 10⁶ cells per milliliter of lysis buffer.

2.9. NA isolation using MPs

The NA extraction procedure was based on the usage of manufactured MPs and isolation kit. 200 µL of lysate was mixed in a test tube with 20 µL of MPs (20 mg · mL⁻¹). The lysis/binding mixture was incubated for 10 min at 25 °C and 500 rpm using a heating and cooling block (Biosan Ltd., Latvia). Subsequently, the MPs were separated by a magnetic platform, and the liquid flow-through was discarded. In the following steps, the MPs-NAs complex was washed with 250 µL of wash buffer I (WBI; pH 6.6, 5 M GITC, 20 mM Tris-HCl, 38 % ethanol), 2 × 500 µL of wash buffer II (WBII; pH 7.5, 20 mM NaCl, 2 mM Tris-HCl, 80 % ethanol) and finally 200 µL of WBII. The washed MPs were dried for 10 min at 55 °C. After thorough evaporation, the samples were well agitated in 40 µL of UltraPure™ DNase/RNase-Free Distilled Water (Thermo Fisher Scientific, Waltham, USA) at 50 °C for 10 min and 500 rpm to elute NAs. The extracted NAs were collected, and MPs were removed afterward.

2.10. UV measurement and agarose gel electrophoresis of isolated NAs

The concentration and purity of isolated NAs were determined spectrophotometrically by NanoDrop™ One/OneC Microvolume UV-Vis Spectrophotometer (Thermo Fisher Scientific, Waltham, MA, USA). The yield of DNA/RNA was expressed as an isolated amount of NAs per mg of MPs. NA integrity was verified using a bleach gel [22]. Samples were separated by 90 V for 35 min in 1 % agarose gel stained by ethidium bromide (0.5 µg · mL⁻¹) supplemented with 1 % bleach. The gel was visualized by Azure c600 from Azure Biosystems (Dublin, CA, USA).

2.11. Densitometric analysis of agarose gel electrophoresis bands

Densitometric analysis of gDNA/RNA bands on agarose gel was determined using ImageJ software. Rectangular boxes were drawn around the individual lines, and the plot lanes option under the Analyze

gels tab was used to obtain intensity profiles. Areas of the profiles corresponding to gDNA and RNA bands on the agarose gel were measured using the magic wand tool.

2.12. Evaluation of the impact of gDNA contamination on RT-qPCR results

Using a First Strand cDNA Synthesis Kit from Roche (Basel, Switzerland), cDNA was transcribed from RNA isolated by MPs-APTES 1/32 %, MPs-APTES 1/2%, MPs-APTES 16 % and MPs-SiO₂. RNA from three independent isolations was used for reverse transcription. According to concentration determined by NanoDrop™ One/OneC Microvolume UV-Vis Spectrophotometer (Thermo Fisher Scientific, Waltham, USA), 500 ng of nucleic acids (NAs: RNA/gDNA) were added to 20 µL reverse transcription reaction containing 4 µL 5X RT Buffer; 2 µL 10 mM dNTP mix; 2 µL 600 mM random hexamer primers; 0.5 µL Protector RNase Inhibitor and 0.5 µL Transcriptor Reverse Transcriptase (RT program: 25 °C for 10 min; 50 °C for 60 min and 85 °C for 5 min). The same amount of NAs (500 ng) was also used for no reverse transcriptase control (NRT) and in the electrophoretic separation by bleach gel. 20 µL of cDNA or NRT was diluted in 380 µL (1:19) of UltraPure™ DNase/RNase-Free Distilled Water (Thermo Fisher Scientific, Waltham, USA) to the final theoretical concentration of 1.25 ng mL⁻¹.

For quantitative real-time polymerase chain reaction (qPCR) was used 5 µL of diluted cDNA/NRT and 4.5 µL of Luna® Universal qPCR Master Mix (New England Biolabs, Ipswich, Massachusetts, USA) with 0.25 µL of 10 µM of forward and reverse primer. Primer sequences shown in Table 1 were designed by PrimerQuest™ Tool (Integrated DNA Technologies, Coralville, USA). Two groups of primer sets were used, the first one enabling qPCR amplification from both cDNA and gDNA (NRT) (*ID1*, *RPLP0*), the second one containing primer sets flanking big intron to avoid gDNA amplification during qPCR setup (*CSRPI*, *MCL1*). qPCR amplification was performed using a real-time instrument qTOWER³ Touch (Analytik Jena, Germany) with the following conditions: initial denaturation at 95 °C for 3 min and subsequent 45 cycles of denaturation at 95 °C for 20 s, annealing and extension at 60 °C for 30 s. The qPCR run was followed by melting curve analysis (MCA: 35 cycles/1 °C increment per 15 s; 60 to 95 °C) to check amplification specificity and determination of melting temperature (T_m) of qPCR products. The qPCR amplicon size was evaluated by gel electrophoresis (2 % agarose gel with EthBr staining; 90 V for 40 min) with Quick-Load® Purple 50 bp DNA Ladder (New England Biolabs, Ipswich, Massachusetts, USA).

2.13. Statistical analysis of RT-qPCR results

The threshold cycles (C_t) determined by qPCRsoft 4.0 (Jena, Germany) are presented in the graphs as mean ± standard deviation from three independent replicates (individual C_t shown in graph). Comparison of C_t between the MPs groups was performed by one-way ANOVA followed by Dunnett's post hoc test (MPs-SiO₂ as the control group) using GraphPad Prism version 8.0.1 (GraphPad Software, CA, USA). T-test was used for the determination of significant differences between C_t values obtained from cDNA and NRT within one MPs group. A p-value less than 0.05 was considered statistically significant.

3. Results and discussion

3.1. Magnetic particles and their characterization

As a first step, magnetite (Fe₃O₄) MPs cores were fabricated following the method reported by Sugimoto and Matijevic [20], which was based on the aging of Fe(OH)₂ gel at elevated temperature. This method allows control over the morphology of the obtained material by adjusting parameters such as temperature, ions presented in the solution, pH, and the type of oxidant used. We scaled up the method to

Table 1
RT-qPCR primer sequences.

Gene Symbol	RefSeq mRNA		Sequence (5'→3')	Size (nt)	Amplicon (bp) cDNA	Amplicon (bp) gDNA (NRT)
ID1	NM_002165.4	Fw	TTGGAGCTGAAGCTCGGAATC	20	148/387	387
	NM_181353.3	Rv	AGCGACACAAGATGCGAT	18		
RPLP0	NM_001002.4	Fw	TCGACAATGGCAGCATCTAC	20	191	191/1282
		Rv	ATCCGTCTCCACAGACAAGG	20		
CSRP1	NM_004078.3	Fw	GGTGTGTCAGAAGACGGTTTA	21	115	5962
		Rv	CACAGTGGTACTGTCCAGATTC	22		
MCL1	NM_021960.5	Fw	GAAAGCTGCATCGAACCATTA	22	105	858
		Rv	AGAACTCCACAACCCTATCC	20		

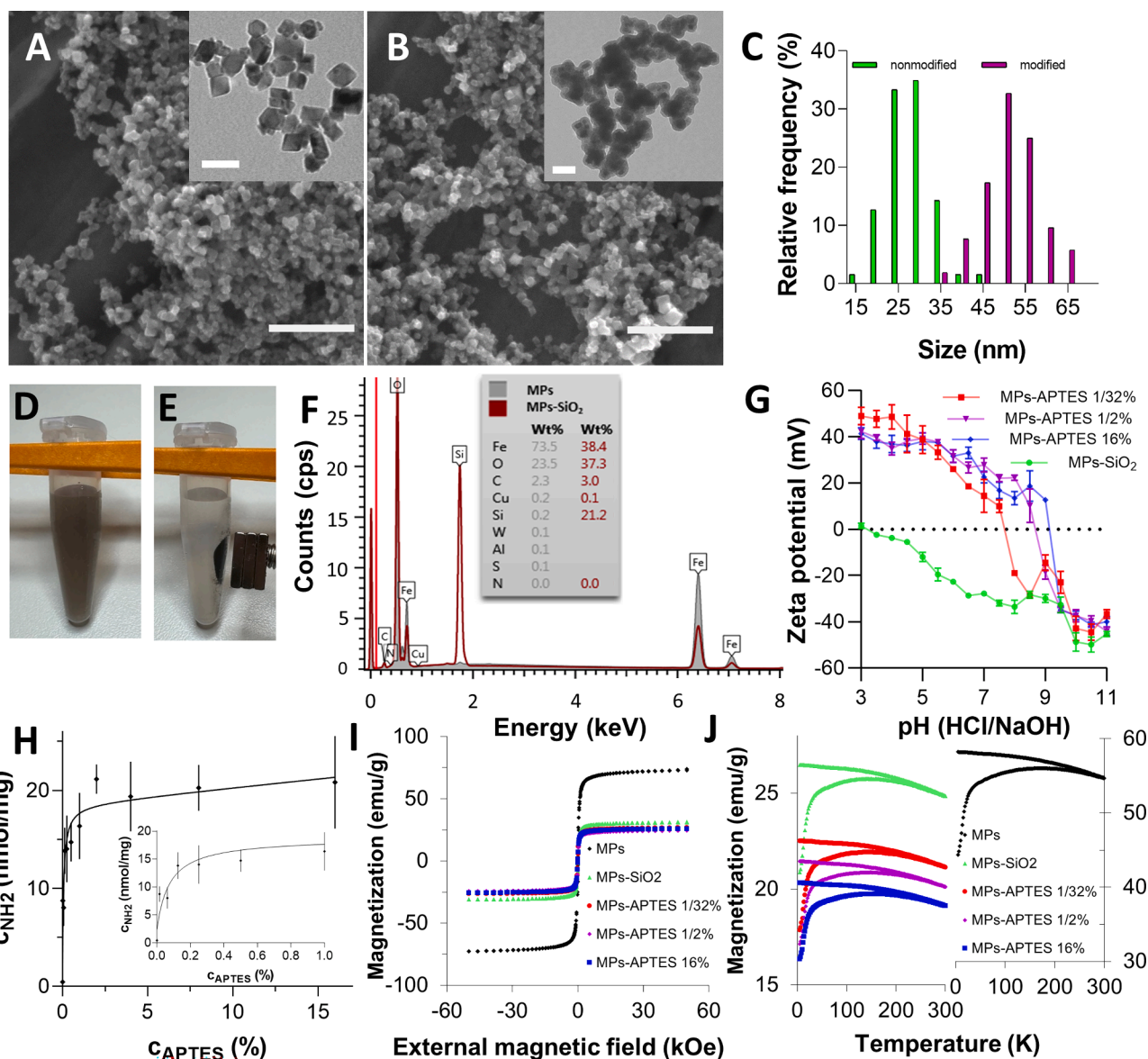


Fig. 1. (A) SEM micrograph of MPs cores (scale bar: 500 nm). The insert shows a TEM micrograph of MPs cores (scale bar: 50 nm). (B) SEM micrograph of MPs-APTES 1% (scale bar: 500 nm). The insert shows a TEM micrograph of MPs-APTES 1% (scale bar: 100 nm). (C) Size distribution of MPs cores (unmodified) and MPs-APTES 1% (modified). (D) Photo of resuspended MPs-APTES 1% ($0.4 \text{ mg} \cdot \text{mL}^{-1}$) and (E) after exposition to the external magnetic field. (F) EDX spectrum of MPs cores (grey line) and MPs-SiO₂. (G) Dependence of zeta potential of MPs-SiO₂, MPs-APTES 1/32%, MPs-APTES 1/2%, MPs-APTES 16% on pH (3–11) in 10 mM KCl. (H) Dependence of amine groups concentration on MPs on the concentration of APTES during MPs modification. The inset shows low APTES concentrations in detail. (I) The dependence of magnetization of MPs cores, MPs-SiO₂, MPs-APTES 1/32%, MPs-APTES 1/2% and MPs-APTES 16% on intensity of applied external magnetic field at 300 K. (J) ZFC and FC measurement of magnetization dependence on temperature of MPs cores, MPs-SiO₂, MPs-APTES 1/32%, MPs-APTES 1/2% and MPs-APTES 16%.

achieve a modified MPs yield of the order of grams. This represents an important achievement as we have fabricated cores necessary for all the following experiments reported in this article in just one batch. The MPs produced according to the procedure described in the *Materials and methods* section are shown in Fig. 1A. This SEM micrograph shows that nanoparticles possess relatively good homogeneity. Further, the generation of undesired antiferromagnetic α -FeOOH (goethite) and γ -FeOOH (lepidocrocite), which would be observed as acicular or twinned particles, was not observed [23]. TEM image provided further MPs morphology details. As can be seen in the figure insert, a significant portion of particles possess rectangular-to-square shapes.

MPs were modified with amine groups using a two step method. At first, MPs were modified with a SiO₂ layer using well established Stöber process [24]. Here, TEOS was hydrolyzed in a mixture of ethanol and water using ammonia as a catalyst. It leads to the condensation of TEOS on the surface of MPs and the creation of a compact SiO₂ layer on them [25]. Analogously to TEOS modification, MPs-SiO₂ were functionalized with amine groups using hydrolysis of APTES. In comparison with MPs core, SEM and TEM images of modified particles (Fig. 1B) show, that the dimensions of particles increased and the sharp edges of MPs cores became rounded. Using electron microscopy, no differences between MPs-SiO₂ and MPs-APTES were observed (see Fig. S1 and Fig. S2 to compare MPs-SiO₂ and selected variants of MPs-APTES).

The sizes of MPs cores and MPs-APTES 1 % were inspected manually from TEM micrographs ($n = 60$). It was calculated that the average size of MPs cores and MPs-APTES 1 % was 28 ± 5.4 nm and 52 ± 6.8 nm, respectively. The inset of Fig. 1B shows, that MP cores are covered with a SiO₂ layer of 12 ± 1.5 nm thickness. The particles size distribution is shown in Fig. 1C. A photo of MPs-APTES 1 % suspension of concentration 0.4 mg mL^{-1} is shown in Fig. 1D. After exposition to an external magnetic field, a pellet of particles (0.4 mg) on the edge of the microtube was created (Fig. 1E).

Elemental composition of MPs cores and MPs-SiO₂ were determined using EDX module of SEM (Fig. 1F). The results showed 73.5, 23.5 and 2.3 wt% (Wt%) of Fe (atomic mass 55.845), O (15.999), and C (12.011), respectively. However, EDX do not provide reliable quantitative results of light elements such as O and C and should be taken with caution. In the case of MPs-SiO₂ EDX spectrum showed 38.4, 37.3, 3.0 and 21.2 wt % of Fe, O, C and Si (atomic mass 28.086), respectively. It confirmed the successful modification of MPs cores with the SiO₂ layer.

Zeta potentials of MPs-SiO₂ and three representative variants covering the whole used APTES concentrations were inspected (pH 3 – 11, Fig. 1G). Regarding MPs-SiO₂, zeta potential is in the vicinity of zero at pH 3. They possess an isoelectric point (IEP) at pH 3.3, where protonated and deprotonated silanol groups are supposed to be balanced. However, in pH > 3.3 deprotonated form (negatively charged) silanol groups prevail and with increasing pH, the zeta potential of MPs-SiO₂ became more and more negative. This zeta potential trend agrees with the zeta potential of SiO₂ particles [26]. MPs-SiO₂ reach moderate colloidal stability (>30 mV) at pH 6.5. Surface zeta potential of all APTES modified particles changed considerably with pH and showed similar behavior as was reported by Wu et al. [27]. In detail, MPs-APTES 1/32 %, MPs-APTES 1/2%, and MPs-APTES 16 % possess high positive zeta potential at low pH. Taking into account the zeta potential of source material (MPs-SiO₂) at this pH, it suggests the presence of NH₂ functional groups on the surface of particles. Zeta potentials decreased with increasing pH and IEP of MPs-APTES 1/32 %, MPs-APTES 1/2%, and MPs-APTES 16 % were 7.7, 8.7 and 9.1, respectively. It suggests, that a higher amount of APTES within the modification solution can functionalize MPs-SiO₂ with a higher amount of amino groups, which replace silanol groups (negative at this pH).

Density of amino groups on the surface of individual APTES modified particles was determined by a simple bind and release method (Fig. 1H). It uses covalent binding of 4-NBA to amino groups through Schiff base creation and subsequent photometric quantification of aldehyde regenerated by hydrolysis from washed samples [28]. The benefit of such a

method is that provides information just about surface groups, which are accessible for reaction and are not sterically hindered [21]. The data showed that only the two lowest concentrations of APTES during synthesis provided significantly lower amounts of surface amine groups than in the case of 1/8 % of APTES within the modification solution ($p < 0.05$). It is evident, that in the described conditions 1/8 % (~0.125 %) of APTES caused particles surface saturation with amino groups. It seems that the used reaction conditions do not provide branched polycondensed structures of APTES as was previously suggested by Liu et al. hence concentration of amino groups is not increasing dramatically [29].

To unveil the magnetic properties of the measured samples, the hysteresis loops and zero field cooling/field cooling (ZFC/FC) magnetization curves were recorded. At room temperature (300 K), the magnetization vs. applied field curve (Fig. 1I) shows significantly lower values of hysteresis parameters (coercivity, remanent magnetization) compared to the values measured at 5 K (Fig. S2) for all measured samples, indicating that the superspins of all magnetic nanoparticles, irrespective of their size in the system, behave in a superparamagnetic manner, fluctuating between the orientations along the easy axis of magnetization favored by the particle magnetic anisotropy. At 5 K, the hysteresis loops display non-zero coercivity and remanence with the values frequently reported for nanoparticle systems of Fe₃O₄ origin. The maximum magnetization values decrease with the surface modification by SiO₂ and APTES, reflecting the diamagnetic or paramagnetic nature of coating surfactants. Nevertheless, the system shows a strong magnetic response as evidenced by reaching the magnetic saturation under small applied magnetic fields.

The passage of the nanoparticle system to the magnetically blocked state is also documented by a broad maximum at the ZFC magnetization curve (see Fig. 1J), corresponding to the average blocking temperature (T_B) of nanoparticles with the most probable size in the assembly. The ZFC and FC magnetization curves separate at the temperature known as the temperature of irreversibility (T_{irr}), which marks the onset of the blocking mechanism of superspins belonging to the largest nanoparticles in the system. The difference between T_{irr} and T_B can be thus interpreted as a quantitative measure of particle size distribution; in our case, the difference between T_{irr} and T_B is quite broad in all measured samples, implying a broader particle size distribution of nanoparticles in the system. Below T_B , the FC magnetization values still continue to increase, evidence that magnetic nanoparticles magnetically interact with each other only very weakly, most probably by dipole-dipole interactions.

3.2. *Nas extraction using MPs with different amount of amino groups on their surface*

Recently, the use of MPs has been considered due to the simplicity of the method, cost-effectiveness, and time-saving properties. Taking into account the physico-chemical conditions, the adsorption of NA on solid surfaces is mainly driven by hydrophobic and electrostatic interactions [30]. Hence, changes in the surface of MPs may have a significant effect on NA adsorption, which is further influenced by binding solution chemical composition, pH, ionic strength, etc. In this study, we compared the quality and quantity of NAs extracted by MPs modified with SiO₂ layer and MPs modified with various amounts of APTES.

The gel indicates that total RNA extracted by all types of MPs is intact with clearly visible sharp bands of 28S and 18S rRNA (Fig. 2A). The gel shows that RNA extracted by MPs-SiO₂ and MPs with low APTES content (1/32 %, 1/16 %, 1/8 %) is contaminated with the gDNA band. This amount of APTES in the reaction solution is probably insufficient to provide full cover of the particles' surface as is evident from particles characterization. It suggests, that the mixture of remaining silanol and amino groups of such particles can bind gDNA in the same way as MPs-SiO₂.

To determine the intensity of the gDNA bands, densitometric analysis was performed using ImageJ software (Fig. 2B). The sample isolated by

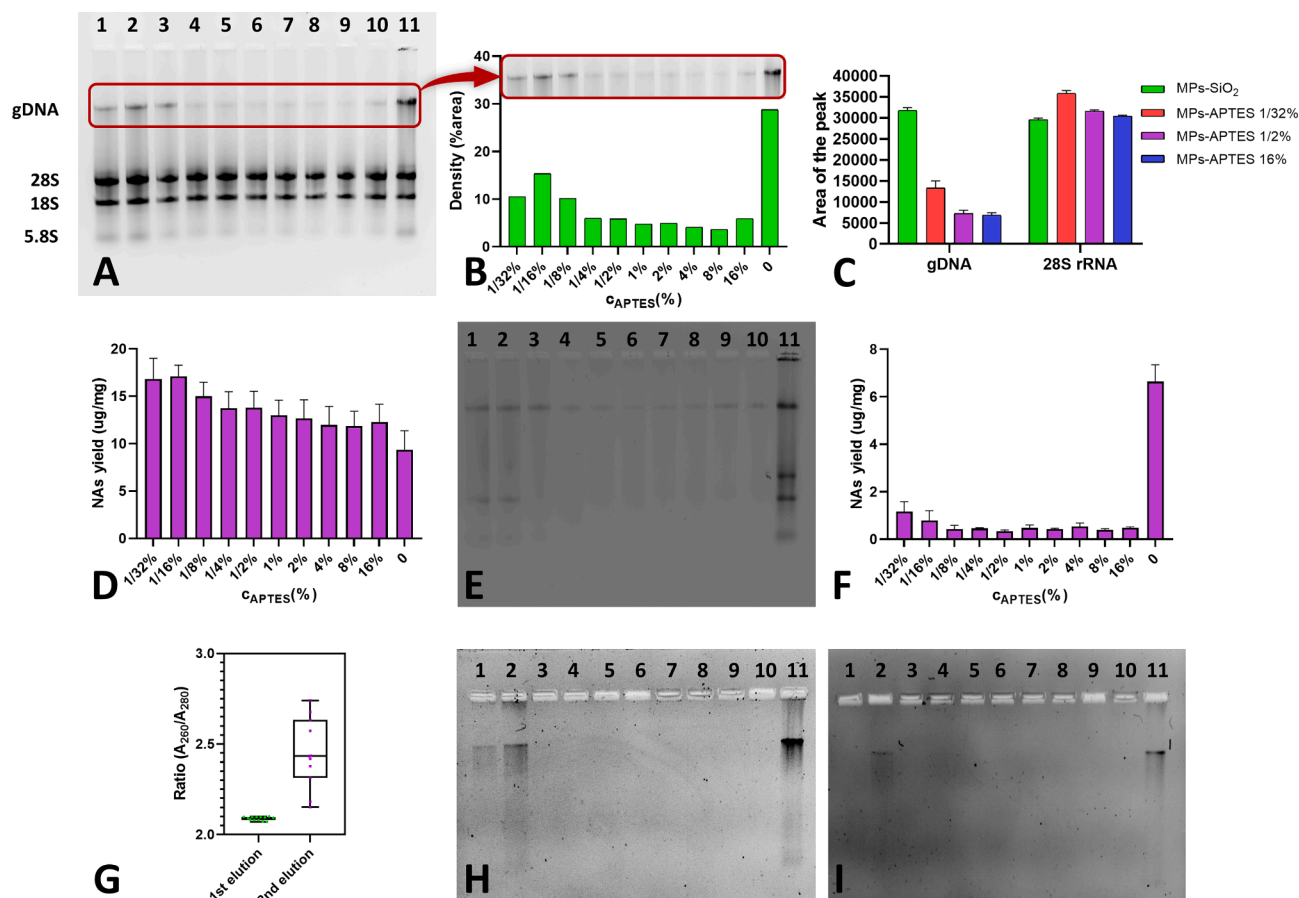


Fig. 2. (A) Agarose gel electrophoresis of first elution of extracted NA using eleven variants of MPs. Lane 1: MPs-APTES 1/32 %; 2: MPs-APTES 1/16 %; 3: MPs-APTES 1/8 %; 4: MPs-APTES 1/4 %; 5: MPs-APTES 1/2 %; 6: MPs-APTES 1 %; 7: MPs-APTES 2 %; 8: MPs-APTES 4 %; 9: MPs-APTES 8 %; 10: MPs-APTES 16 %; 11: MPs-SiO₂. The same series of samples is seen in Fig. 2EHI. (B) Densitometric analysis (% area) of gDNA bands and comparative analysis of gDNA and (C) 28S rRNA bands. (D) The graph shows the concentration of extracted NAs in the first elution as mean ± standard deviation from four independent replicates. (E) The gel shows the integrity and quality of extracted NAs in the second elution. (F) Graphs indicate the concentration of extracted NAs in the second elution from two replicates and (G) the A₂₆₀/A₂₈₀ ratio of extracted NAs in the first and second elution. Gel electrophoresis results of the first (H) and second (I) NA re-isolation.

MPs-SiO₂ contains a gDNA band that represents 29 % of the total area, while the sample isolated by low APTES content (1/32 %, 1/16 %, 1/8 %) contains gDNA bands of approximately 10, 15, 10 %, respectively. In the case of higher APTES concentrations (1/4 % – 16 %) during particles modification, the intensities of the gDNA bands were at a similar level around 5 %.

We conducted a comparison between the gDNA and 28S rRNA bands in the NAs isolated by MPs-SiO₂, MPs-APTES 1/32 %, MPs-APTES 1/2 %, and MPs-APTES 16 % by calculating their bands intensities ratio (Fig. 2C). Our findings show that the gDNA band in the sample isolated with MPs-SiO₂ is 7 % more intense than the 28S rRNA band. On the other hand, samples isolated using MPs modified with APTES showed more intense bands for 28S rRNA than gDNA. We observed that MPs with the lowest amount of APTES (MPs-APTES 1/32 %) had a 63 % more intense 28S rRNA band than gDNA. Similarly, MPs-APTES 1/2 % and MPs-APTES 16 % had a 77 % more intense 28S rRNA band compared to gDNA. The mentioned ratios correspond to the amount of amino groups present on the surface of the particles. MPs with higher APTES content and the described procedure selectively isolates RNA without the presence of gDNA. This is a significant advantage for many techniques used in gene expression analysis e.g. for the isolation of RNA from bacteria, which is often contaminated with gDNA [31]. In this case, an additional gDNA removal step must be used and the RNA solution must be treated with DNase. However, this treatment increases the cost of the isolation process (e.g., TURBO™ Dnase by Invitrogen costs 555 €/5,000 units). The procedure is not 100 % effective for the removal of gDNA, and the

resulting RNA is often of lower quality and purity, which can negatively affect subsequent analyses.

In Fig. 2D, the effectiveness of NAs isolations were expressed as the amount of isolated NAs per mg of used magnetic particles. The average NAs' concentration in eluate obtained by MPs-APTES (138 ng μL^{-1} ~ 13.81 $\mu\text{g mg}^{-1}$) was higher than NAs' concentration obtained by MPs-SiO₂ by 48 % (94 ng $\cdot \mu\text{L}^{-1}$ ~ 9.36 $\mu\text{g mg}^{-1}$). The highest concentration of NAs was obtained by MPs-APTES 1/16 % (171 ng $\cdot \mu\text{L}^{-1}$ ~ 17.10 $\mu\text{g mg}^{-1}$). However, the isolated RNA was contaminated with gDNA. As the amount of APTES in the modification solution increases, the concentration of isolated RNA is almost identical. This may correspond to the reaching of amine-grafting capacity of the particle surface hence. As mentioned above, saturation of the particle surface with amino groups was achieved at 1/8 % (~0.125 %) APTES conditions. Lower NAs concentrations were determined when isolated using MPs with higher amounts of APTES (4 %–16 %). The optimal MPs for RNA isolation in relation to concentration appear to be MPs-APTES 1/2 %, which isolates a sufficient amount of RNA (138 ng $\cdot \mu\text{L}^{-1}$ ~ 13.78 $\mu\text{g mg}^{-1}$), without the significant presence of gDNA.

To release all bound NAs from the particle surface in the elution step is a fundamental requirement of isolation protocols based on silica matrixes. If all NAs were not released from the particles' surface in the first elution, an additional elution step would have to be added to the isolation protocol. This extra step could potentially affect the quality and integrity of the isolated NA, and, in addition, the secondary elution could contain particles whose magnetic behavior can be influenced by

changes of solution chemistry. Their presence in the eluate may lead to inhibition of reverse transcription [32]. Moreover, the addition of a second elution would be disadvantageous for the possibility of automating the isolation process. MPs modified with APTES release all the NAs from the sample in the first elution, whereas the MPs-SiO₂ release a significant part of the NAs in the second elution (Fig. 2E). The results showed that the concentration of NAs in the second elution obtained by MPs-SiO₂ was 66 ng · μL⁻¹ (~6.6 μg · mg⁻¹) and NAs obtained by MPs with low APTES content (1/32 %, 1/16 %) was around 10 ng · μL⁻¹ (~1 μg · mg⁻¹) (Fig. 2F). Particles with higher amounts of APTES (1/8% – 16 %) released all RNA already in the first elution. The NA concentration in the second elution was nearly zero (4 ng · μL⁻¹ ~ 0.4 μg · mg⁻¹). From this point of view, it is more convenient to use MPs-APTES than MPs-SiO₂ for NAs extraction. Taking into account MPs-APTES, MPs-SiO₂ zeta potentials and buffers composition, the elution data suggests that hydrophobic interaction plays an important role in MPs-SiO₂ to NAs interaction, and one step is not sufficient to fully rehydrate all presented NAs. However, in the case of the interaction between MPs-APTES and NAs, it appears that the shift in pH from 6.6 (the pH of the lysis buffer) to 7.5 (the pH of the elution buffer) can disrupt the electrostatic attraction, which is the dominant force at play here.

The purity of extracted NAs is usually described by the ratio of absorbance at 260 nm and 280 nm ($A_{260/280}$), where a value 2.0 indicates highly pure RNA [33]. The mentioned ratio around 1.8 suggests predominant presence of DNA within sample. The results showed, that the $A_{260/280}$ ~ 2.0 in the first elution and isolated NAs was considered as pure (Fig. 2G). The purity of extracted NAs by MPs-SiO₂ and released in the second elution was 2.1 and $A_{260/280}$ of the released NAs in the second elution by MPs-APTES was 2.3 – 2.7.

Another important parameter in the isolation of NAs using MPs is the binding capacity of the specific particle surface. The basic requirement is that the MPs are able to bind all NAs from the sample. We used the samples, from which NAs had been already isolated, and performed the first and the second NAs re-isolation from them. MPs-APTES were able to bind all RNA from the sample in the first isolation process, no bands or smears are visible on the gel (Fig. 2HI). The light smear of gDNA can be found in samples isolated in the first re-isolation by MPs with low amounts of APTES (1/32, 1/16 %). In contrast, a relatively intense gDNA band can be observed in samples isolated in the first re-isolation by MPs-SiO₂. This band is also evident in the second re-isolation (Fig. 2I).

The binding mechanism between NAs and silica and other solid surfaces is still a topic of debate. It has been reported that electrostatic interaction including hydrogen bonding between NAs and silanol groups as well as hydrophobic interaction play a role depending on the conditions [9,10]. Regarding the hydrophobic interaction, it should be noted that although perfect SiO₂ (known as quartz) is hydrophilic due to the presence of surface siloxane bonds, different types of silanol groups (isolated, vicinal, or geminal silanol) increase its hydrophobicity [34]. Although the water contact angle of nanoparticles cannot be obtained experimentally, the reported water contact angles for quartz, hydroxylated quartz, and aminated quartz plates were < 10°, 24.8°, and 72.3°, respectively [35]. Katevatis et al. experimentally demonstrated that hydrophobic interactions play a major role over hydrogen and ionic interactions in holding the DNA-chaotropic salt-silica complex together [36]. Double-stranded NAs have a hydrophobic interior due to the presence of purines and pyrimidines. However, their dispersibility in aqueous solutions is mediated by a charged exterior (phosphate backbone). Chaotropic agents (urea, etc.) and chaotropic salts (including guanidinium and thiocyanate ions) are able to influence non-covalent interactions within biomolecules and between biomolecules and their environment. Although chaotropic agents such as urea disrupt the hydrogen bond network between water molecules, thus destabilising the hydrophobic aggregates of biomolecules and allowing them greater structural freedom, chaotropic salts shield electrostatic interactions. The effects of chaotropes on proteins are well known, but few studies have

focused on their effects on NAs [37–39]. For example, Sarkar et al. suggested contradictory effects of the non-ionic chaotrope, urea, and the ionic chaotrope, guanidinium cation, on dsDNA structure [40]. They reported that guanidinium cation increases the stability of Watson-Crick base pairs and urea vice versa. In the present study, we used the ionic chaotrope GITC, which contains two strong chaotropic ions, guanidinium cation and thiocyanate anion, which have been reported to effectively denature DNA origami [41]. However, our results showed that isolated gDNA remained in double-stranded form even in the presence of 4.5 M GITC. We suggest that the higher affinity of the highly hydrophobic surface of MPs-APTES for RNA than for gDNA is due to the single-stranded structure of RNA, where hydrophobic nitrogen bases are more exposed than in DNA, despite the presence of diverse secondary structures. It is worth noting that the interaction of negatively charged silanol groups of MPs-SiO₂ with negatively charged DNA phosphates is not favourable at the pH we used (pH 6.6) and is probably mediated by guanidinium cation [42]. Here GITC reduces electrostatic repulsive forces, promotes hydrophobic interactions and mediates the formation of hydrogen bonds [10]. We do not expect a significant role for ionic interaction between gDNA/RNA and the MPs-APTES surface, as suggested by the successful elution of NAs from MPs-APTES by changing the ionic strength of the solution [42].

3.3. Dependence of NA isolation efficiency on the quantity of MPs in the reaction

A critical point in the NAs extraction process is to find the optimal amount of MPs to isolate all the NAs from the sample without residual sample contamination in just one procedure. A higher quantity of applied MPs in NA extraction does not necessarily mean a larger specific surface area of MPs for NA binding. In addition, an overload of MPs may reduce the quality of isolated NA and may inhibit downstream applications. Conversely, a lower quantity of MPs may not provide a large enough specific surface area to extract all the NAs from the sample. The effects of MPs amounts were studied for MPs-SiO₂ and MPs-APTES 1/2 %, based on the above results. The following amounts of MPs 800 μg, 400 μg, 200 μg, 100 μg, 50 μg and 25 μg were added to the isolation process.

The results showed that the optimal amount of MPs, from the yield point of view, for NAs isolation from 1 · 10⁶ cells was 400 μg and 200 μg using MPs-SiO₂ with an NA yield of 7.8 μg in both cases. In case of MPs-APTES 1/2 %, 400 μg was an optimal amount in the tested scheme with an NA yield of 10.7 μg (Fig. 3ABC). [43,44] A significant decrease of NA yield is observed with higher amounts of MPs using MPs-SiO₂, a slight decrease is also observed with MPs-APTES 1/2 %. Min et al. (2014) reported that NA extraction yields by MPs decrease with increasing MPs quantity after reaching the saturation point [45]. At higher amounts of MPs, such a trend in NA isolation yields could be observed due to the excessive amounts of magnetic supports, which can complicate NAs elution [45,46]. The graph demonstrates that the MPs-APTES 1/2 % can isolate a higher amount of NAs compared to the MPs-SiO₂. Moreover, it can isolate NAs even when extremely low amounts of MPs are used (50 μg, 25 μg), which is a significant advantage as it reduces the possibility of downstream applications being inhibited due to the large number of MPs remaining in the eluate (Fig. 3C). In addition, the whole process could be more cost-effective for routine use in the laboratory or for usage in automated NA isolation systems. When 50 μg of MPs-APTES 1/2 % were used, the isolation efficiency was four times higher than the efficiency with the same amount of MPs-SiO₂. When using the lowest amount of MPs-APTES 1/2 % (25 μg), the isolation efficiency was reduced by 58 %, resulting in a final NA yield of 4.6 μg. Using the lowest amount of MPs-SiO₂ (25 μg) resulted in a 95 % decrease with an NA yield of 0.4 μg. The discussed trend is even more visible in the Fig. 3D, where the NAs yields per mg of used particles are shown. In the case of 100 μg of particles used per isolation and more, both MPs-SiO₂ and MPs-APTES 1/2 % exhibited comparable results. However, a lower amount (50 and

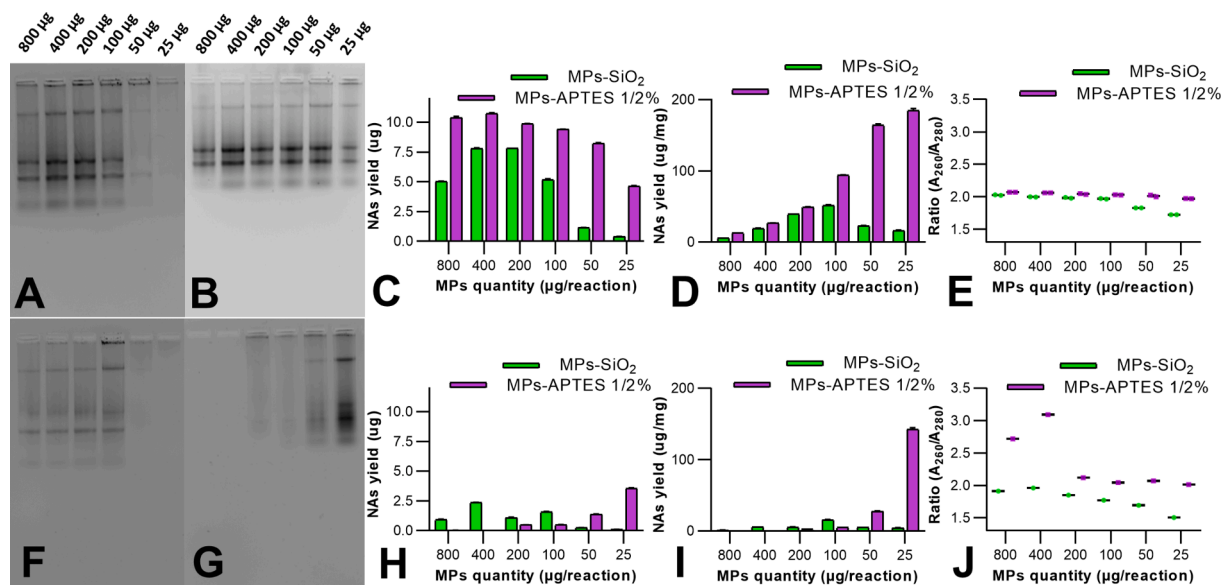


Fig. 3. Agarose gel electrophoresis results of NA extraction using different contents of MP-SiO₂ (A) and MP-APTES 1/2 % (B) in the extraction process (µg per isolation). Lane 1: 800 µg; 2: 400 µg; 3: 200 µg; 4: 100 µg; 5: 50 µg; 6: 25 µg. The same series of samples is seen in Fig. 3FG. Diagrams show the mean ± standard deviation of total yield (C), yield per mg of MPs (D) and purity (E) of extracted NA from two replicates. Gel electrophoresis results show re-isolation of NA using different contents of MP-SiO₂ (F) and MP-APTES 1/2 % (G) in the extraction process. The diagrams show the total yield (H), yield per mg of MPs (I) and purity (J) of extracted NA in re-isolation from two replicates.

25 µg) of MP-APTES 1/2% showed a massive isolation effectivity increase. On the contrary, a lower amount of MP-SiO₂ in the isolation mixture caused isolation effectivity to decrease.

Using the data above, adsorption capacity of MP-APTES 1/2% was calculated to be 26.8 mg · g⁻¹. Chen et al. reported sorption capacity 27.86 mg · g⁻¹ ($A_{260/280} \sim 1.84$) of hemoglobin modified magnetic nanocomposite for plasmid DNA [43]. In case of RNA, Sun et al. reported adsorption capacity 7.7 mg · g⁻¹ of silica coated magnetic particles [44]. Polydopamine modified magnetic nanoparticles showed excellent adsorption capacity 161 mg · g⁻¹ for DNA from bacterial lysate [47]. However, the quality of extracted DNA was compromised ($A_{260/280} \sim 1.80$).

The purity of all NA samples extracted with MP-APTES 1/2% is within the acceptable range ($A_{260/280} \sim 1.97\text{--}2.07$), whereas NAs isolated with MP-SiO₂ are considered pure ($A_{260/280} \sim 1.97\text{--}2.02$), only when NAs were isolated with larger amounts of particles (800 µg–100 µg) (Fig. 3E). The $A_{260/280}$ ratio of the isolated NA with lower amounts of MP-SiO₂ (50 µg–25 µg) is approximately 1.73 – 1.82, indicating a predominance of gDNA and almost no RNA in the eluate.

In this study, we used the samples from which NAs were already isolated and performed NA re-isolation to determine if the NAs remaining within samples can be isolated, or are not able to interact with the particles at all. The gel and graph indicate that a minimal concentration of NAs remained in the sample when MP-SiO₂ (800 µg–100 µg) were used (Fig. 3FG). No bands are visible on the gel when isolating NAs with a lower amount of particles MP-SiO₂ (50 µg–25 µg). This amount of TEOS-modified MPs is too low to extract NA from the sample. In contrast, a larger amount of MP-APTES 1/2 % bound all NAs in the first isolation, and no NA molecules were already present in the sample for re-isolation. As the amount of MP-APTES 1/2 % in the reaction decreases, the concentration of NA in the re-isolation increases, confirming that MP-APTES 1/2% possess decent NAs binding ability even at low particles concentrations. (Fig. 3H). Fig. 3I confirmed the trend mentioned above. Taking into account all these results, a very interesting phenomenon emerges. Although APTES modified magnetic particles are able to bind NAs at high and even at low concentrations, SiO₂ modified particles' binding effectivity below critical concentration decreases dramatically (100 µg per isolation in this experimental setup).

The purity of NAs extracted by different amounts of MP-APTES 1/2 % and MP-SiO₂ in the second elution was outside the accepted range, which is since a significant amount of NA was already released in the first elution (Fig. 3J).

3.4. Effect of different cell numbers on NA extraction

The literature mostly discusses the minimum number of cells required for NA isolation in good quality for RT-PCR. This is important when dealing with samples with a limited amount of the target molecule. NEB's guidelines for the purification of RNA from cultured mammalian cells report that RNA can be purified from as few as 100 cells. Surface modified MPs are generally known to be able to extract NAs from very small amounts of samples due to the complex linkages they enable. Hypothetically, different modifications of MPs allow the formation of differently sized specific surfaces. In terms of the different surfaces of MPs, it is important to understand how much NAs they are able to bind to their surface. Specifically, we need to know the maximum capacity of a specific particle surface. In order to determine this, we conducted a study where NAs were isolated from different numbers of cells. An identical amount of MPs (400 µg) was used for each experiment, based on the results mentioned above.

Choosing the optimal sample quantity can have a big impact on the quality of the separated sample. Too many NAs loaded into the gel can influence the migration of the sample; an overloaded fragment runs slower and may therefore appear larger than it actually is. The excessive amount of NAs loaded into the gel may also affect the band intensity and the separated sample may appear degraded due to the presence of a visible smear. The result demonstrates an overloaded gel, in which 8 µl of the extracted NAs has been applied (Fig. 4A). This means that $8.2 \cdot 10^3$ ng of NAs was loaded into the gel in the isolated NAs with the highest concentration. Although the gel is saturated, we can still assess the differences in the concentrations of NAs present in the samples qualitatively. The intensity of the bands on the gel is consistent with the number of cells from which NAs were extracted. Hence, the most intense bands are visible in NAs that were extracted from $5 \cdot 10^6$ cells, whereas the weakest bands are produced by samples extracted from 10^6 cells. This pattern is similar for samples extracted by MP-SiO₂ and MP-

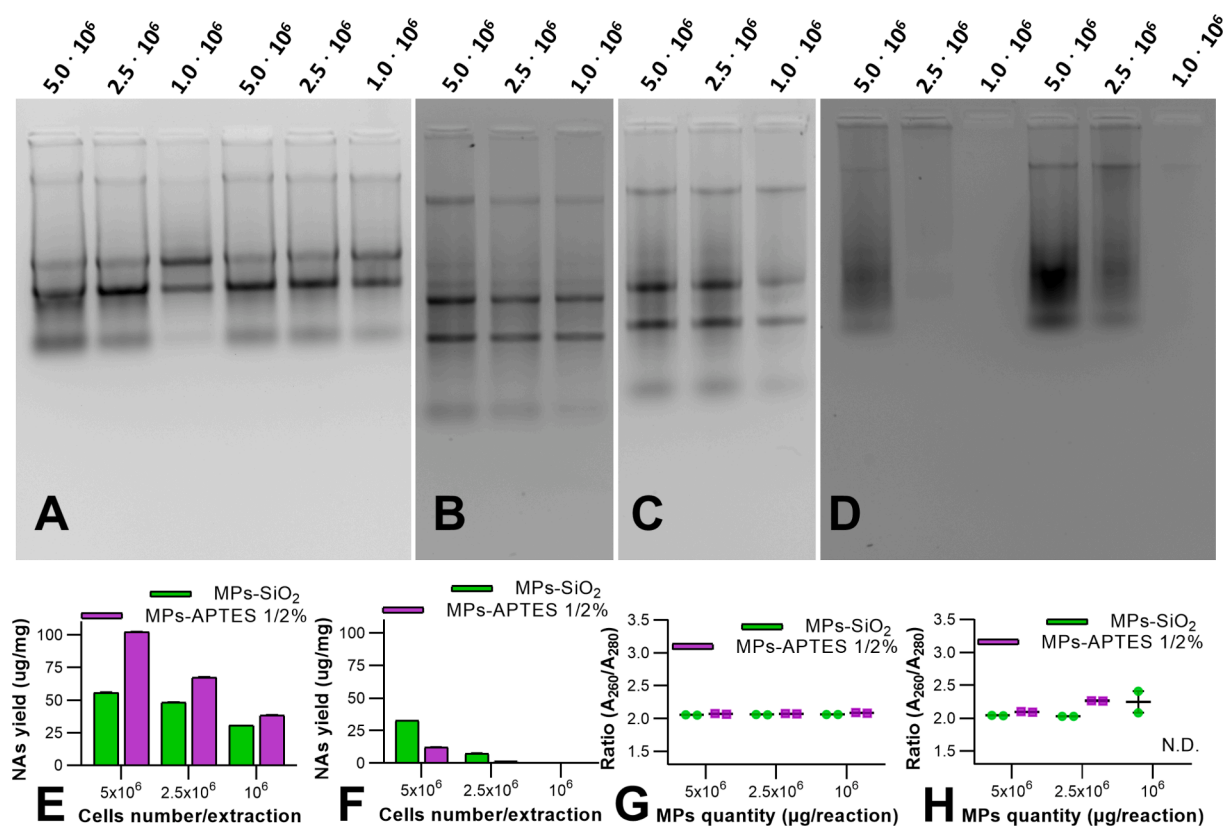


Fig. 4. Gel electrophoresis results of NA extraction using MP-APTES 1/2 % (lane 1 – 3) and MP-SiO₂ (lane 4 – 6) from various numbers of cells (1,4: 5 · 10⁶ cells; 2,5: 2.5 · 10⁶ cells; 3,6: 1 · 10⁶ cells) (A). Samples are numbered from left to right. 10 µl of each sample was loaded into an agarose gel containing 8 µl of extracted NA and 2 µl of loading buffer (60 % glycerol, 40 % RNase-free water). Gels for more detailed visualization of the quality and integrity of RNA isolated through MP-APTES 1/2 % (lane 1: 5 · 10⁶ cells; 2: 2.5 · 10⁶ cells; 3: 1 · 10⁶ cells) (B) and MP-SiO₂ (lane 1: 5 · 10⁶ cells; 2: 2.5 · 10⁶ cells; 3: 1 · 10⁶ cells) (C). 10 µl of each sample was loaded into an agarose gel containing 8 µl of sample mixture (2 µl of extracted NA and 6 µl of RNase-free water) with 2 µl of loading buffer (60 % glycerol, 40 % RNase-free water). Gel electrophoresis results show NA re-isolation with different cell numbers using MP-APTES 1/2 % (lane 1 – 3) and MP-SiO₂ (lane 4 – 6) (D). The diagrams show the yield of extracted NAs from the first isolation (E), from the re-isolation (F), and its purity obtained from the first isolation (G) and the re-isolation (H). (N.D. = not detected).

APTES 1/2 %. Furthermore, the same trend can be observed with gels that are not saturated (Fig. 4BC). 2 µl of NAs were loaded into the gel, which is equivalent to approximately 2 · 10³ ng NAs in the highest concentration sample. The individual bands are more visible on the gel, which is not overloaded.

The graph indicates that the concentration of NAs extracted from a sample of 5 · 10⁶ cells was 55 % lower when isolated with MP-SiO₂ than when isolated with MP-APTES 1/2 % (Fig. 4E). This suggests that particles modified with just the SiO₂ layer have a lower binding capacity, which leads to earlier saturation compared to MPs with an additional APTES layer. The saturation point, when all binding sites were filled, was reached by MP-SiO₂ when NAs were extracted from 5 · 10⁶ cells. MP-APTES 1/2 % have a larger binding capacity which allows them to isolate a significant number of NAs from an excessive number of cells. The concentration of NAs isolated using MP-APTES 1/2 % is consistent with the number of cells from which NAs were extracted. As the number of cells in the sample increases (from 10⁶ to 5 · 10⁶), the concentration of isolated NAs also increases (from 38.47 µg · mg⁻¹ ~ 384.7 ng · µL⁻¹ to 102.1 µg · mg⁻¹ ~ 1021 ng · µL⁻¹). The specific binding surface of MPs with both SiO₂ and APTES layers is probably larger because even when extreme amounts of cells were used, the surface was not completely saturated.

In order to determine the saturation of the specific particle surface in the first isolation, it was necessary to perform a re-isolation for this experiment. Both types of MPs were able to isolate all NAs from the sample with the lowest number of cells in the first isolation (Fig. 4DF). However, the particles' surface became saturated when NAs were

isolated from the largest number of cells. This trend was observed for both MP-APTES 1/2 % and MP-SiO₂. The data showed that the concentration of NAs extracted from 5 · 10⁶ cells using MP-SiO₂ was 324 ng · µL⁻¹ (32.47 µg · mg⁻¹), which is 62 % higher than the extraction using MP-APTES 1/2 % (Fig. 4F). Similarly, when NAs were extracted from a middle number of cells (2.5 · 10⁶), the concentration of NAs was approximately 75 ng · µL⁻¹ (7.54 µg · mg⁻¹) using MP-SiO₂, which is up to 80 % higher than the extraction using MP-APTES 1/2 %. Furthermore, when NAs were isolated using MP-APTES 1/2 % from 5 · 10⁶ and 2.5 · 10⁶ cells, almost all NAs were extracted. The results show that MP-SiO₂ were unable to extract a large amount of NAs from 5 · 10⁶ and 2.5 · 10⁶ cells. A significant quantity of NAs remained in the sample. This may be due to the smaller binding capacity of MPs modified only by a SiO₂ layer.

All NA samples extracted in the first isolation using MP-SiO₂ and MP-APTES 1/2% are in the purity range. The A₂₆₀/A₂₈₀ ratios reached a satisfying value of 2.05 – 2.09 for all samples together (Fig. 4G). The NAs isolated in re-isolation are also within an acceptable range of purity except the NAs isolated from 2.5 · 10⁶ and 1 · 10⁶ cells using MP-APTES 1/2 % (Fig. 4H). This is due to the binding of all NAs from the sample to the particle surface in the first isolation.

3.5. Assessment of gDNA contamination prior to RT-qPCR by bleach gel image analysis

The purity and integrity of isolated RNA represent key aspects for obtaining accurate RT-qPCR results and contaminated or degraded RNA

can hinder this process. gDNA, commonly co-isolated during RNA extraction, is also considered as unwanted contaminant and can lead to overestimation of gene expression, particularly when the target mRNA has no introns (e.g. prokaryotes) or has several processed pseudogenes in the genome.

All the NA samples isolated by MPs with different surface modifications, including MPs modified with 1/32 % APTES, 1/2 % APTES, 16 % APTES, and MPs without APTES modification (0 % = MPs-SiO₂), exhibited similar average A_{260/A280} ratios close to 2 (2.06 ± 0.03, 2.07 ± 0.2, 2.08 ± 0.02, and 2.06 ± 0.04, respectively), suggesting that samples are primarily composed of RNA species. According to these ratios was not possible to evaluate the extent of gDNA contamination or severity of RNA degradation. Therefore, we used bleach gel to check the presence of gDNA and the integrity of RNA before performing RT-qPCR.

Unlike in previous bleach gels where equal volumes of crude NAs samples were immediately evaluated after isolation, an equal amount of NAs (500 ng) was used for electrophoretic separation (Fig. 5A). Upon evaluation of RNA integrity and quality, no signs of aberrant degradation were observed in the any of tested samples. Subsequently, the extent of gDNA contamination was assessed by comparing the intensities of distinct gDNA bands using image analysis in ImageJ software. Visualization of bands via plot profile analysis (Fig. 5B) revealed the highest gDNA intensity (~decrease in average gray value) in NA samples isolated by MPs without APTES modification (0 % = MPs-SiO₂). Densitometric analysis indicated that all NA samples isolated by MPs with APTES surface modification contained significantly lower gDNA levels (p < 0.001) compared to MPs-SiO₂ extracts (Fig. 5C). MPs modified with the lowest APTES concentration (1/32 %) exhibited 53.5 ± 19.9 % gDNA content relative to MPs-SiO₂ (100 ± 2.7 %). In addition, a greater reduction in gDNA contamination was observed in MPs-APTES 1/2 % and MPs-APTES 16 % samples containing only 17.9 ± 2.0 % and 19.7 ± 1.2 % gDNA, respectively, compared to NAs lacking APTES modification. In other words, NAs species isolated by MPs modified by 1/32 % 1/2%, and 16 % APTES contained approximately 1.9 times, 5.9 times, and 5.1 times less gDNA, respectively, than MPs-SiO₂ NAs extracts.

It is important to take into account that actual gDNA contamination of NA extracts may be higher because some of the DNA fragments may not be visible due to the limit of detection of bleach (agarose) gels with EthBr staining. Furthermore, the visible smear above and below the main gDNA band may contain DNA fragments of various sizes. Densitometric quantification of this type of gDNA contamination could be

compromised, due to the possibility that the smear below the major band may contain RNA, such as not fully denatured rRNAs. To address these potential issues, subsequent experiments were conducted to compare the overall gDNA contamination of NA extracts using qPCR by analyzing samples without reverse transcriptase (NRT). Furthermore, the impact of gDNA on gene expression analysis was also assessed. Primer sets that enable amplification only from cDNA in a defined qPCR program were employed. Additionally, primers that may generate the amplicons from both NA species cDNA and also from gDNA were utilized.

3.6. Evaluation of the impact of NAs extracts on RT-qPCR using cDNA-specific primers

To ensure the reliability of gene expression profiles assessed by RT-qPCR, the reverse transcription (RT) and quantitative real-time polymerase chain reaction (qPCR) steps must be unaffected by the impurities in RNA extracts. The A_{260/230} ratio serves as an indicator of the most common RNA contaminants introduced during the RNA isolation process including chaotropic salts (e.g. GITC, GuHCl), detergents (Triton X-100, Tween 20), phenol, EDTA, or ethanol. However, some contaminants such as GuHCl, can only be detected in RNA isolates at high concentrations that are not normally presented after elution, so contamination of RNA samples by commonly used guanidine salt often remains undetected. MPs alone also represent potential unwanted RNA contaminants that could influence RT-qPCR results and are usually not detectable by conventional spectrophotometric measurements (A_{260/280} and A_{260/230} ratios). To determine if the tested NA extracts, in addition to varying amounts of gDNA, also contained other undetected factors with a potential negative impact on downstream RNA applications, we compared average threshold cycle (Ct) values determined by RT-qPCR.

In order to avoid the influence of potential gDNA amplicons on Ct values, primer sets for two target genes (*CSRPI* = 115 bp; *MCL1* = 105 bp) were designed to span long introns (5847 bp and 753 bp). The specificity of designed primers was validated by the separation and visualization of the qPCR amplicons on 2 % agarose gel (Fig. 6B) and also by melting curve analysis (MCA) following the qPCR program (Fig. 6C). Unsurprisingly, there were no qPCR amplicons, Ct values or melting temperatures (T_m) in of the case of NRT samples, making it highly unlikely that the gDNA contamination could directly affect the Ct values obtained from cDNA amplifications.

Therefore, the Ct values shown in Fig. 6A could serve to determine

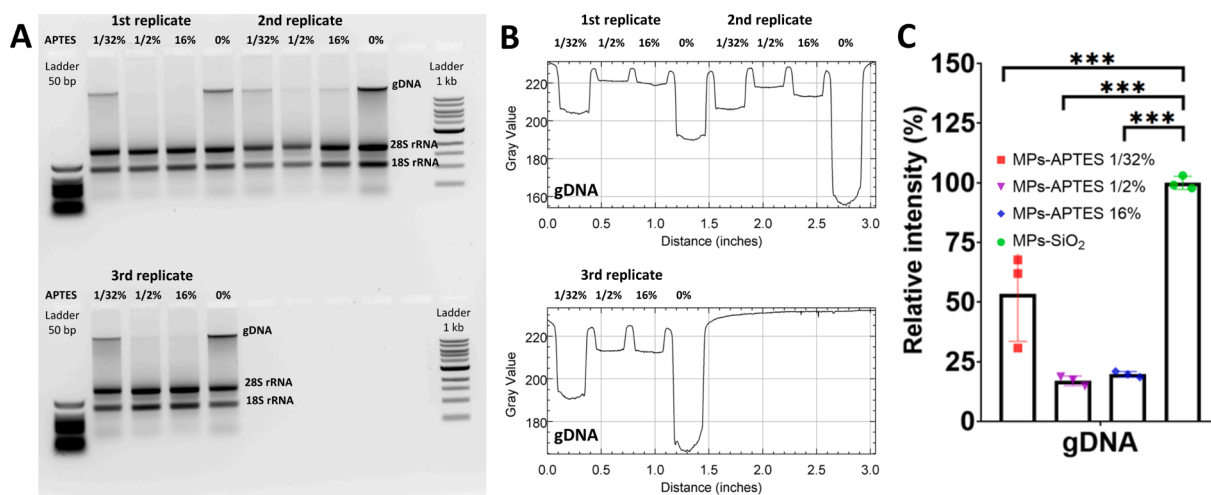


Fig. 5. Evaluation of gDNA contamination of NAs isolates before RT-qPCR. Electrophoretic patterns of NAs isolated by MPs with 1/32 %, 1/2 %, 16 %, and 0 % APTES (MPs-SiO₂) surface modification (A). Plot profile of gDNA bands determined by image analysis – ImageJ (grayscale 0–255, 0 = black, 255 white) (B). Comparison of average gDNA band intensities isolated by MPs modified by APTES normalized to band intensities of MPs-SiO₂ isolates (0 % APTES) (C). (***: p < 0.001).

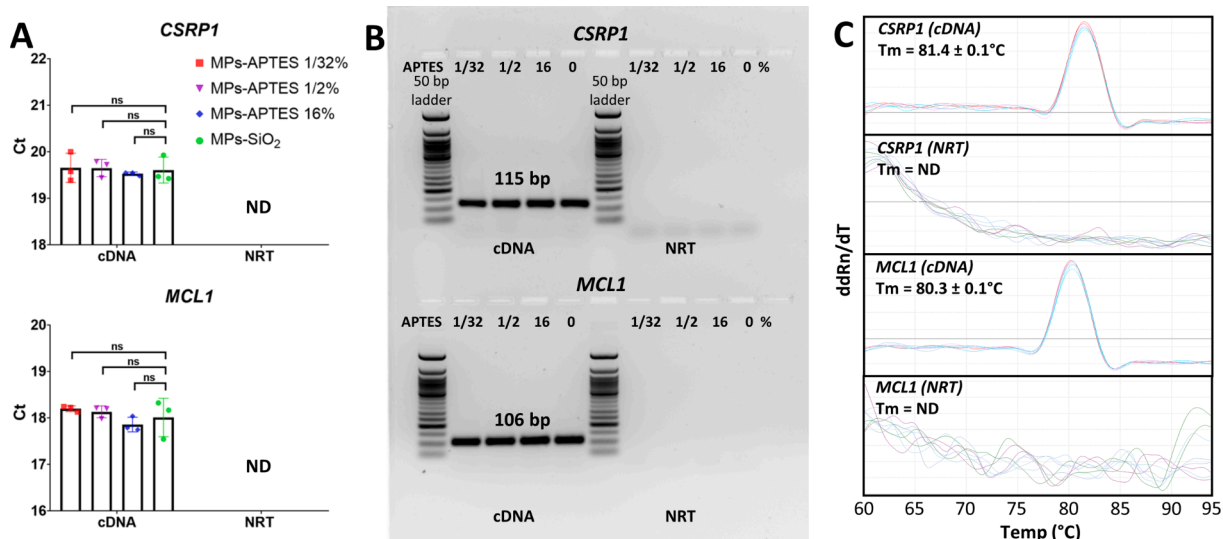


Fig. 6. Effect of NAs samples isolated by MPs with different APTES modifications on RT-qPCR using cDNA-specific primers for *CSRP1* and *MCL1*. Comparison of threshold cycles (C_t) obtained from NAs isolated by APTES-modified MPs with MPs without APTES surface modification (A). Visualization of cDNA and NRT qPCR amplification products on 2 % agarose gel (B). Melting temperature (T_m) of cDNA and NRT qPCR amplicons (C). (ns: not significant; ND: not determined).

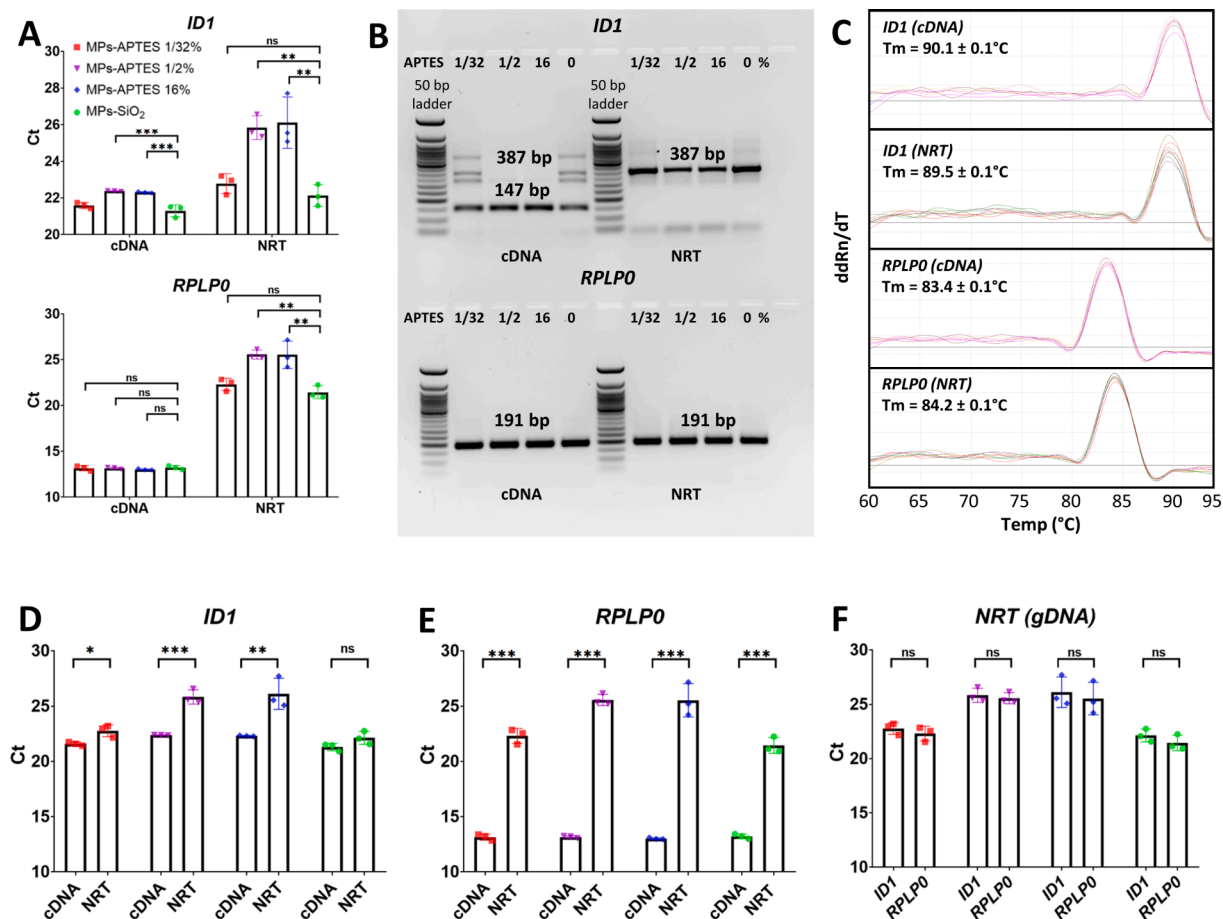


Fig. 7. Assessment of the influence of gDNA contamination on RT-qPCR results and estimation of the extent of gDNA contamination by qPCR using non-cDNA unique primer sets for *ID1* and *RPLP0*. Comparison of C_t values determined by RT-qPCR (cDNA) and qPCR (extent of gDNA contamination) using NAs isolated by APTES-modified MPs with MPs without APTES surface modification (MPs-SiO₂) (A). Visualization of cDNA and NRT qPCR amplification products on 2 % agarose gel (B). Melting temperatures (T_m) of cDNA and NRT qPCR amplicons (C). MPs-specific comparison between C_t values acquired from cDNA and gDNA utilizing primers for *ID1* and E) *RPLP0* (D). MPs-specific evaluation of differences between *ID1* and *RPLP0* NRT C_t values (F). (*: $p < 0.05$; **: $p < 0.01$; ***: $p < 0.001$; ns: not significant).

CSRPI and *MCL1* gene expression. Finally, we compared average Ct values obtained from RNA samples isolated by MPs without APTES (MPs-SiO₂) with Ct values determined from extracted RNAs by MPs with varying amounts of APTES surface modifications (1/32 %, 1/2 %, 16 %). Comparison of Cts between the MPs groups was performed by one-way ANOVA followed by Dunnett's post hoc test (MPs-SiO₂ as the control). For both genes, there were no significant differences between Cts determined from MPs-SiO₂ isolates and MPs-APTES 1/32 %, MPs-APTES 1/2 %, and MPs-APTES 16 %. This was evident from Ct values (mean ± SD) calculated from three independent experiments, and two technical replicates (Ct values for *CSRPI*: 19.61 ± 0.28 vs. 19.66 ± 0.31, 19.65 ± 0.19 and 19.53 ± 0.04, Ct values for *MCL1*: 18.01 ± 0.41 vs. 18.20 ± 0.06, 18.13 ± 0.13 and 17.86 ± 0.16 respectively). These findings indicated that RNA isolated by MPs without or with APTES modification reached a comparable quality, and was likely to be free from any significant impurities that could compromise RT-qPCR results utilizing cDNA-specific primers.

3.7. Evaluation of the impact of NAs extracts on RT-qPCR and qPCR results using primers generating amplicons from both cDNA and gDNA

Following the previous experiment setup, the Ct values obtained from cDNA synthesized from NA samples isolated by MPs with or without APTES modifications were compared (Fig. 7A). Two primer sets targeting genes *ID1* and *RPLPO* with different basal expressions were used. For highly expressed *RPLPO*, there were no significant differences between average Ct values from MPs-SiO₂ extracts and Ct values obtained from NAs isolated by MPs with 1/32 %, 1/2%, and 16 % APTES modifications (cDNA Ct values: 13.22 ± 0.21 vs. 13.15 ± 0.28, 13.16 ± 0.10 and 13.02 ± 0.07, respectively). These observations were consistent with RT-qPCR results using cDNA-specific primers for *CSRPI* and *MCL1*.

However, this trend was not observed in the case of *ID1*, the gene with considerably lower basal expression (T47D: *ID1* = 70.5 nTPM vs. *RPLPO* = 4636.2 nTPM; <https://www.proteinatlas.org>). Significantly lower Ct values (Fig. 7A) were determined from NA samples isolated by MPs-SiO₂ compared to MPs modified by 1/2 % and 16 % APTES (cDNA Ct values: 21.29 ± 0.33 vs. 22.37 ± 0.02 and 22.30 ± 0.03, respectively). However, there were no significant differences in Ct values between samples isolated by MPs-SiO₂ and those modified by 1/32 % APTES (21.29 ± 0.33 vs. 21.58 ± 0.17, respectively). The densitometric analysis (Fig. 5C) and qPCR analysis of NRT samples (Fig. 7A) revealed that NA samples extracted by MPs-SiO₂ contained the highest amount of gDNA, followed by MPs with 1/32 % APTES. These findings, in conjunction with the detection of non-specific products likely originating from gDNA in *ID1* cDNA amplicons (Fig. 7B), suggest that gDNA contamination may have contributed to the observed decrease in Cts following RT-qPCR, potentially leading to an overestimation of *ID1* expression. Additionally, the rate of gDNA contamination of MPs-SiO₂ isolates was so high that NRT samples reached almost the same Ct values as cDNA samples (Fig. 7D) utilizing *ID1* primers (22.13 ± 0.59 vs. 21.29 ± 0.33, $p = 0.099$). Moreover, after conducting the melting curve analysis (MCA), it was observed that both the NRT and cDNA *ID1* amplicons displayed similar peak shapes and melting temperatures (Fig. 7C). This made it challenging to determine which amplicon predominantly influenced the final Ct values in the RT-qPCR. The Ct values from NRT using *ID1* and *RPLPO* targeting primers did not show significant differences (Fig. 7F). However, *RPLPO* gene expression was less affected compared to *ID1*, as the cDNAs for *RPLPO* outnumbered the gDNA contaminants (Fig. 7E). These results indicated that gDNA contamination of RNAs isolated by MPs-SiO₂ or by MPs-APTES 1/32 % could adversely affect RT-qPCR analysis, especially for target genes with low expression levels and no option to design cDNA-specific primers. While the expression profile of *RPLPO*, a housekeeping gene with high basal expression, seemed unbiased by the amount of gDNA contamination, other commonly used reference housekeeping genes like *ACTB* or

GAPDH could be negatively influenced due to the presence of dozens of pseudogenes in the human genome [48].

In addition to evaluating the impact of gDNA on RT-qPCR, we sought to assess the extent of gDNA contamination by comparing Ct values in NRT samples. The lowest Ct values, indicating the highest gDNA contamination, were found in NRTs prepared from NA samples isolated by MPs-SiO₂ (Fig. 7A). There were no significant differences between threshold cycles obtained by amplification of *ID1* or *RPLPO* targets in NRT samples (Fig. 7E). The amount of gDNA contamination in NA samples extracted by APTES-modified MPs was estimated by normalization of APTES Ct values to MPs-SiO₂ Cts ($\Delta Ct_{\text{norm}} = Ct_{\text{SiO}_2\text{NRT}} - Ct_{\text{APTESNRT}}$). The mean Ct differences for MPs-APTES 1/32 %, MPs-APTES 1/2%, and MPs-APTES 16 % were -0.8, -3.9, and -4.0 respectively. This corresponds to approximately 1.7 times, 15.1 times, and 16.4 times lower gDNA contamination than in NA extracts isolated by MPs-SiO₂. Although the estimated differences determined by qPCR were higher than in the case of densitometric analysis, there were significant negative correlations (Spearman rank) between gDNA band intensities *ID1* NRT Ct values ($r = -0.86$, $p < 0.001$) and *RPLPO* NRT Ct values ($r = -0.89$, $p < 0.001$). According to these results, the primer set targeting the *RPLPO* gene could be used for the estimation of leftover gDNA contamination by qPCR using NRT controls.

4. Conclusion

The present study focuses on the isolation of DNA and RNA from cell line lysate using amine-modified magnetic nanoparticles. A series of iron oxide MPs with different amounts of surface amine groups were prepared. Amine groups were grafted onto iron oxide MPs modified with a SiO₂ layer using the Stöber method. Deep characterization of material morphology, zeta potentials, amine group concentrations, and magnetic properties revealed cores of 28 ± 5.4 nm with uniform SiO₂ (12 ± 1.5 nm). Chemical determination of reactive amine group concentrations on fabricated MPs-APTES showed saturation behaviour within the applied APTES concentrations (0.13 %–16 %) and individual particles possessed from 8.0 to 20.8 nmol of amine groups per mg of particles. Increasing the amount of amine groups replacing silanol groups on the surface of the particles resulted in a decrease in their maximum magnetisation and an increase in their isoelectric points. As expected, amine-modified particles exhibited completely different surface zeta potential dependence on pH compared to MPs-SiO₂ (IEP 3.3).

Gel electrophoresis combined with photometric determination of NA concentrations and RT-qPCR was used to evaluate the isolation properties of MPs NA from the human breast cancer cell line T47D. Compared to SiO₂-modified particles, which are currently accepted as the standard in this field, amine-modified particles showed increased yields of isolated NAs. However, depletion of gDNA was observed, demonstrating preferential isolation of RNA by APTES-modified particles. In addition, elution of NAs from the particles was impaired in the case of MPs-SiO₂ and particles with a low amount of amine groups. Significant differences in isolation efficiency were observed between MPs-SiO₂ and MPs-APTES 1/2 %. In the experimental setup used, 400 µg of both particles gave the highest yields. Although doubling the dose of MPs-SiO₂ caused a decrease in the yield of NAs, this effect was not observed in the case of MPs-APTES 1/2 %. This makes MPs-SiO₂ not ideal for the isolation of NAs' from undefined samples. In terms of efficacy, MPs-SiO₂ reached an optimal ratio of NAs' yield to the applied amount of MPs at 100 µg per isolation. Both decrease and increase decreased the isolation efficiency. However, MPs-APTES 1/2 % showed a constant increase in isolation efficacy with a decrease in sample dose and constant product purity.

NAs isolated by APTES-modified MPs contained significantly lower amounts of gDNA than MP-SiO₂ extracts, as was demonstrated by densitometric analysis and qPCR. RT-qPCR analysis revealed that gDNA-contaminated NAs from MP-SiO₂ isolations may lead to overestimation of gene expression levels, particularly when targeting lowly expressed

genes without the possibility to design cDNA-specific primers. The NAs extracted by MPs with 1/2 % or 1/16 % APTES surface modification exhibited the lowest gDNA contamination and provided consistent RT-qPCR results using both cDNA-specific and non-specific primers. Overall, MPs with 1/2 % APTES appeared to be the optimal tool for isolating high-quality RNA, which can be used to determine gene expression by RT-qPCR.

CRedit authorship contribution statement

Petra Vopařilová: Investigation, Conceptualization, Validation, Writing – original draft. **Zbyněk Šplíchal:** Conceptualization, Formal analysis, Investigation, Writing – original draft, Writing – review & editing. **Pavel Švec:** Investigation. **Pavel Kulich:** Investigation. **Ondřej Malina:** Investigation, Writing – original draft. **Michal Otyepka:** Funding acquisition, Writing – review & editing. **Ondřej Zítka:** Funding acquisition, Writing – review & editing. **Jiří Kudr:** Conceptualization, Funding acquisition, Writing – review & editing, Project administration.

Declaration of competing interest

The authors declare that they have no known competing financial interests or personal relationships that could have appeared to influence the work reported in this paper.

Data availability

Data will be made available on request.

Acknowledgment

We acknowledge the financial support of Grant No. TN02000017 from the Technology Agency of the Czech Republic (National Centre for Biotechnology in Veterinary Medicine), and the ERDF “Multidisciplinary research to increase application potential of nanomaterials in agricultural practice” No. CZ.02.1.01/0.0/0.0/16_025/0007314. Petra Vopařilová would like to acknowledge the financial support from the Internal grant agency of the Faculty of AgriSciences, Mendel University in Brno (No. IGA24-AF-IP-066). Ondřej Malina and Michal Otyepka would like to thank the Research Infrastructure NanoEnvicZ, supported by the Ministry of Education, Youth and Sports of the Czech Republic under Project No. LM2023066.

Appendix A. Supplementary material

Supplementary data to this article can be found online at <https://doi.org/10.1016/j.seppur.2024.129788>.

References

- [1] S.C. Tan, B.C. Yiap, DNA, RNA, and protein extraction: the past and the present, *J. Biomed. Biotechnol.* 10 (2009).
- [2] L.S. Toni, A.M. Garcia, D.A. Jeffrey, X. Jiang, B.L. Stauffer, S.D. Miyamoto, C. C. Sucharov, Optimization of phenol-chloroform RNA extraction, *MethodsX* 5 (2018) 599–608.
- [3] M.O. Hammad, Simplified protocol modification of TRIzol method for extraction of high-quality RNA yield from RNase-rich rat pancreas, *Process Biochem.* 130 (2023) 464–471.
- [4] T. Dang, S. Bodaghi, F. Osman, J. Wang, T. Rucker, S.-H. Tan, A. Huang, D. Pagliaccia, S. Comstock, I. Lavagi-Craddock, K.R. Gadhave, P. Quijia-Lamina, A. Mitra, B. Ramirez, G. Uribe, A. Syed, S. Hammado, I. Mimou, R. Campos, S. Abdunour, M. Voeltz, J. Bae, E. Dang, B. Nguyen, X. Chen, N. Siddiqui, Y. T. Hsieh, S. Abu-Hajar, J. Kress, K. Weber, G. Vidalakis, A comparative analysis of RNA isolation methods optimized for high-throughput detection of viral pathogens in California’s regulatory and disease management program for citrus propagative materials, *Front. Agron.* 4 (2022).
- [5] P. Chomczynski, N. Sacchi, The single-step method of RNA isolation by acid guanidinium thiocyanate–phenol–chloroform extraction: twenty-something years on, *Nat. Protocols* 1 (2006) 581–585.
- [6] R.M. McCormick, A solid-phase extraction procedure for DNA purification, *Anal. Biochem.* 181 (1989) 66–74.
- [7] C.-S. Chang, H.-S. Ni, S.-Y. Suen, W.-C. Tseng, H.-C. Chiu, C.P. Chou, Preparation of inorganic–organic anion-exchange membranes and their application in plasmid DNA and RNA separation, *J. Membr. Sci.* 311 (2008) 336–348.
- [8] S. Mirna Lorena, P.C. Cynthia, A.R. Maria Isabela, V.M. Pamela, R.H. Gabriela, B. Jorge, G. Mariano, Nucleic acids isolation for molecular diagnostics: present and future of the silica-based DNA/RNA purification technologies, *Sep. Purif. Rev.* 52 (2023) 193–204.
- [9] B. Shi, Y.K. Shin, A.A. Hassanali, S.J. Singer, DNA binding to the silica surface, *J. Phys. Chem. B* 119 (2015) 11030–11040.
- [10] W.-Y. Chen, D. Matulis, W.-P. Hu, Y.-F. Lai, W.-H. Wang, Studies of the interactions mechanism between DNA and silica surfaces by Isothermal Titration Calorimetry, *J. Taiwan Inst. Chem. Eng.* 116 (2020) 62–66.
- [11] F. Poly, C. Chenu, P. Simonet, J. Rouiller, L. Jocteur, Monrozier, differences between linear chromosomal and supercoiled plasmid DNA in their mechanisms and extent of adsorption on clay minerals, *Langmuir* 16 (2000) 1233–1238.
- [12] S. Isailovic, H.-W. Li, E.S. Yeung, Adsorption of single DNA molecules at the water/fused-silica interface, *J. Chromatogr. A* 1150 (2007) 259–266.
- [13] T.H. Nguyen, M. Elimelech, Plasmid DNA adsorption on silica: kinetics and conformational changes in monovalent and divalent salts, *Biomacromolecules* 8 (2007) 24–32.
- [14] C.A. Scholes, D.P. Millar, M.L. Gee, T.A. Smith, Resonance energy-transfer studies of the conformational change on the adsorption of oligonucleotides to a silica interface, *J. Phys. Chem. B* 115 (2011) 6329–6339.
- [15] M. Beld, C. Sol, J. Goudsmit, R. Boom, Fractionation of nucleic acids into single-stranded and double-stranded forms, *Nucleic Acids Res.* 24 (1996) 2618–2619.
- [16] P. Cai, Q. Huang, X. Zhang, Microcalorimetric studies of the effects of MgCl₂ concentrations and pH on the adsorption of DNA on montmorillonite, kaolinite and goethite, *Appl. Clay Sci.* 32 (2006) 147–152.
- [17] P. Oberacker, P. Stepper, D.M. Bond, S. Höhn, J. Focken, V. Meyer, L. Schelle, V. J. Sugrue, G.-J. Jeunen, T. Moser, S.R. Hore, F. von Meyenn, K. Hipp, T.A. Hore, T. P. Jurkowski, Bio-On-Magnetic-Beads (BOMB): Open platform for high-throughput nucleic acid extraction and manipulation, *PLoS Biol.* 17 (2019) e3000107.
- [18] J. Kudr, Y. Haddad, L. Richtera, Z. Heger, M. Cernak, V. Adam, O. Zitka, Magnetic nanoparticles: from design and synthesis to real world applications, *Nanomaterials* 7 (2017) 243.
- [19] J. Kudr, B. Klejdus, V. Adam, O. Zitka, Magnetic solids in electrochemical analysis, *TrAC Trends Anal. Chem.* 98 (2018) 104–113.
- [20] T. Sugimoto, E. Matijevic, Formation of uniform spherical magnetite particles by crystallization from ferrous hydroxide gels, *J. Colloid Interf. Sci.* 74 (1980) 227–243.
- [21] Y. Sun, F. Kunc, V. Balhara, B. Coleman, O. Kodra, M. Raza, M. Chen, A. Brinkmann, G.P. Lopinski, L.J. Johnston, Quantification of amine functional groups on silica nanoparticles: a multi-method approach, *Nanoscale Adv.* 1 (2019) 1598–1607.
- [22] P.S. Aranda, D.M. LaJoie, C.L. Jorczyk, Bleach gel: a simple agarose gel for analyzing RNA quality, *Electrophoresis* 33 (2012) 366–369.
- [23] H.T. Cui, W.Z. Ren, P. Lin, Y. Liu, Structure control synthesis of iron oxide polymorph nanoparticles through an epoxide precipitation route, *J. Exp. Nanosci.* 8 (2013) 869–875.
- [24] W. Stöber, A. Fink, E. Bohn, Controlled growth of monodisperse silica spheres in the micron size range, *J. Colloid Interf. Sci.* 26 (1968) 62–69.
- [25] O. Malay, I. Yilgor, Y.Z. Menciloglu, Effects of solvent on TEOS hydrolysis kinetics and silica particle size under basic conditions, *J. Sol-Gel Sci. Technol.* 67 (2013) 351–361.
- [26] P. Xu, H. Wang, R. Tong, Q. Du, W. Zhong, Preparation and morphology of SiO₂/PMMA nanohybrids by microemulsion polymerization, *Colloid Polym. Sci.* 284 (2006) 755–762.
- [27] Z. Wu, H. Xiang, T. Kim, M.-S. Chun, K. Lee, Surface properties of submicrometer silica spheres modified with aminopropyltriethoxysilane and phenyltriethoxysilane, *J. Colloid Interf. Sci.* 304 (2006) 119–124.
- [28] F. Kunc, N. Nirmalanathan-Budau, B. Rühle, Y. Sun, L.J. Johnston, U. Resch-Genger, Interlaboratory comparison on the quantification of total and accessible amine groups on silica nanoparticles with qNMR and optical assays, *Anal. Chem.* 93 (2021) 15271–15278.
- [29] Y. Liu, Y. Li, X.-M. Li, T. He, Kinetics of (3-Aminopropyl)triethoxysilane (APTES) Silanization of Superparamagnetic Iron Oxide Nanoparticles, *Langmuir* 29 (2013) 15275–15282.
- [30] D.K. Chattoraj, A. Mitra, Adsorption of DNA at solid–water interfaces and DNA–surfactant binding interaction in aqueous media, *Curr. Sci.* 97 (2009) 1430–1438.
- [31] C. Paska, I. Barta, O. Drozdovszky, B. Antus, Elimination of bacterial DNA during RNA isolation from sputum: Bashing bead vortexing is preferable over prolonged DNase treatment, *PLoS One* 14 (2019) e0214609.
- [32] Y. Bai, Y. Cui, G.C. Paoli, C. Shi, D. Wang, X. Shi, Nanoparticles affect PCR primarily via surface interactions with PCR components: using amino-modified silica-coated magnetic nanoparticles as a main model, *ACS Appl. Mater. Interf.* 7 (2015) 13142–13153.
- [33] L. Wang, J.P. Stegemann, Extraction of high quality RNA from polysaccharide matrices using cetyltrimethylammonium bromide, *Biomaterials* 31 (2010) 1612–1618.
- [34] H. Zhang, Z. Xu, W. Sun, Y. Zhu, D. Chen, C. Zhang, Hydroxylation structure of quartz surface and its molecular hydrophobicity, *Appl. Surf. Sci.* 612 (2023) 155884.
- [35] J. Wu, H. Wang, A. Zhu, F. Long, Adsorption kinetics of single-stranded DNA on functional silica surfaces and its influence factors: an evanescent-wave biosensor study, *ACS Omega* 3 (2018) 5605–5614.

- [36] C. Katevatis, A. Fan, C.M. Klapperich, Low concentration DNA extraction and recovery using a silica solid phase, *PLoS One* 12 (2017) e0176848.
- [37] R.A. Curtis, J. Ulrich, A. Montaser, J.M. Prausnitz, H.W. Blanch, Protein-protein interactions in concentrated electrolyte solutions - Hofmeister-series effects, *Biotechnol. Bioeng.* 79 (2002) 367–380.
- [38] T. Wang, X.W. Wang, Y.C. Long, G.M. Liu, G.Z. Zhang, Ion-specific conformational behavior of polyzwitterionic brushes: exploiting it for protein adsorption/desorption control, *Langmuir* 29 (2013) 6588–6596.
- [39] M.W. Qoronfleh, L.K. Hesterberg, M.B. Seefeldt, Confronting high-throughput protein refolding using high pressure and solution screens, *Protein Expr. Purif.* 55 (2007) 209–224.
- [40] S. Sarkar, P.C. Singh, Alteration of the groove width of DNA induced by the multimodal hydrogen bonding of denaturants with DNA bases in its grooves affects their stability, *Biochimica et Biophysica Acta (BBA) - General Subjects* 1864 (2020) 129498.
- [41] M. Hanke, N. Hansen, E. Tomm, G. Grundmeier, A. Keller, Time-dependent DNA origami denaturation by guanidinium chloride, guanidinium sulfate, and guanidinium thiocyanate, *Int. J. Mol. Sci.* (2022).
- [42] L.J. Bruce, T. Sen, Surface modification of magnetic nanoparticles with alkoxy silanes and their application in magnetic bioseparations, *Langmuir* 21 (2005) 7029–7035.
- [43] X.W. Chen, Q.X. Mao, J.W. Liu, J.H. Wang, Isolation/separation of plasmid DNA using hemoglobin modified magnetic nanocomposites as solid-phase adsorbent, *Talanta* 100 (2012) 107–112.
- [44] N. Sun, C. Deng, Y. Liu, X. Zhao, Y. Tang, R. Liu, Q. Xia, W. Yan, G. Ge, Optimization of influencing factors of nucleic acid adsorption onto silica-coated magnetic particles: Application to viral nucleic acid extraction from serum, *J. Chromatogr. A* 1325 (2014) 31–39.
- [45] J.H. Min, M.-K. Woo, H.Y. Yoon, J.W. Jang, J.H. Wu, C.-S. Lim, Y.K. Kim, Isolation of DNA using magnetic nanoparticles coated with dimercaptosuccinic acid, *Anal. Biochem.* 447 (2014) 114–118.
- [46] X. Xie, X. Nie, B. Yu, X. Zhang, Rapid enrichment of leucocytes and genomic DNA from blood based on bifunctional core-shell magnetic nanoparticles, *J. Magn. Mater.* 311 (2007) 416–420.
- [47] Y. Wang, X. Ma, C. Ding, L. Jia, pH-responsive deoxyribonucleic acid capture/release by polydopamine functionalized magnetic nanoparticles, *Analytica Chimica Acta* 862 (2015) 33–40.
- [48] Y. Sun, Y. Li, D. Luo, D.J. Liao, Pseudogenes as weaknesses of ACTB (Actb) and GAPDH (Gapdh) used as reference genes in reverse transcription and polymerase chain reactions, *PLoS One* 7 (2012) e41659.